Nanoscale

Accepted Manuscript

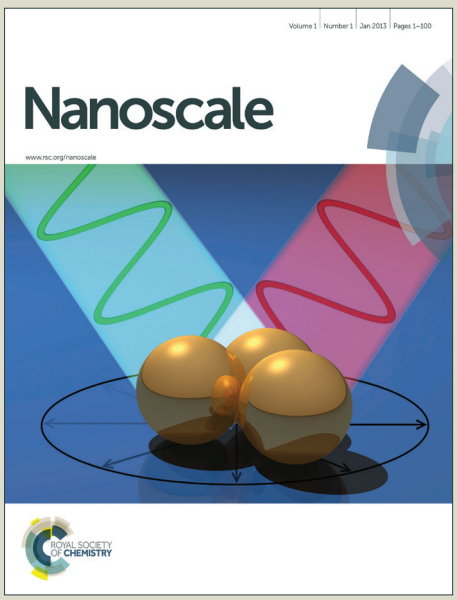

ROYAL SOCIETY OF CHEMISTRY

www.rsc.org/nanoscale

Journal Name

RSCPublishing

ARTICLE

Dye-free near-infrared surface-enhanced Raman scattering nanoprobes for bioimaging and high-performance photothermal cancer therapy

FfCite this: DOI: 10.1039/x0xx00000x

Received ooth January 2012,
Accepted ooth January 2012

DOI: 10.1039/x0xx00000x

www.rsc.org/

Zhiming Liu,* Binggang Ye, Mei Jin, Haolin Chen, Huiqing Zhong, Xinpeng Wang and Zhouyi Guo*

Near-infrared surface-enhanced Raman scattering (NIR SERS) imaging is now a promising molecular imaging technology due to its narrow spectral bandwidth, low background interference and deep imaging depth. In this work, we reports a novel strategy for fabrication of NIR SERS nanoprobes without using any expensive and highly toxic organic dyes. Multifunctional conducting polymer (CP) materials, serving as both the biocompatible surface coatings and the NIR-active reporters, are directly fabricated on the surface of gold nanorods (GNRs) *via* facile oxidative polymerization. The dye-free NIR SERS nanoprobes (GNR-CPs) exhibit good structural stability, well biocompatibility and intriguing NIR SERS activity. GNR-CPs also show extraordinary NIR photothermal transduction efficiency, indicating the potential for cancer therapy. The applications of GNR-CPs as new types of theranostic agents for NIR SERS imaging and high-performance photothermal therapy are accomplished *in vitro* and *in vivo*.

Introduction

Near-infrared (NIR) optical nanoprobes have garnered overwhelming attention in recent years as multimode therapeutic agents for both biomedical imaging and photothermal tumor ablation. In the case of optical molecular imaging, surface-enhanced Raman scattering (SERS) imaging is emerging as an attractive alternative to fluorescence-based techniques with extraordinary signal intensity and specificity. The narrow spectral bandwidth and resistance to photobleaching and autofluorescence make SERS a powerful bio-analytical tool for non-invasive single-cell analysis, rapid diagnosis of diseases, as well as biomedical imaging.[1-7]

Typical NIR SERS nanoprobes often consist of three elements: noble metal substrate, Raman active molecules and the biocompatible surface coating. Dyes which are intensively active at NIR wavelengths are often adopted as the Raman active reporter molecules, and the NIR SERS nanotags are fabricated by directly binding of the dyes to the metal surface.[8-12] However, the electrostatic interaction based metal-dye system suffers from the structural instability, especially in the physiological environments. Sulfur chemistry in NIR dyes allows the close interaction between metal surface and the dye molecule, but the chemical process is inevitable to be complex and high cost. Strong cytotoxicity is another disadvantage that restrict the applications of dye-based SERS nanotags in biomedicine. Surface coating with biocompatible hydrophilic polymers can remarkably improve the biocompatiblity of metal-dye system, in the case of which thiolated polyethylene glycol (PEG-SH) is commonly used.[6, 12] While competitive binding of PEG-SH and dye to the metal surface will weaken the SERS activity of nanoprobes. Moreover, the PEGylated nanostructures are ineligible for NIR photothermal therapy because of their unstable spatial structures that often suffer from morphology change (melting) under high-power NIR irradiation.[13] The steric structures of therapeutic nanotags can be protected by silication *via* sophisticated synthesis routes.[14-17] However, the dye incorporation is still uncontrollable during the silication process, and the silica shell thickness should be well controlled to acquire the optimal SERS signals.[14]

Herein, a novel and facile strategy is proposed for preparing ultrasensitive NIR SERS nanoprobes, in which new types of NIR-active polymers are employed as both the Raman reporter and the biocompatible surface coating. This dye-free strategy renders a low-cost, simple and easy-manipulated fabrication procedure of SERS tags. Conducting polymer (CP) materials, the new NIR photothermal therapeutic agents,[18-23] have served as novel coating materials of metal nanoparticles using a one-pot oxidative polymerization. The CP-coated nanoparticles exhibit reduced cytotoxicity, improved structural stability and enhanced photothermal energy conversion efficiency.[24-28] We here exploit the CP-coated metal nanoparticles as the ultrasensitive NIR SERS labels for tumor detection and imaging, since the Raman signals of CP molecules can be remarkably enhanced by the metal nanostructures after CP-coatings generation under NIR laser excitation. These new styles of NIR SERS nanotags also possess extraordinary photothermal transduction efficiency, which endows them with therapeutic potentials for tumor imaging and photothermal therapy.

Results and discussion

Synthesis and characterization of SERS nanoprobes

Gold nanorods (GNRs) show many advantages as attractive substrates for NIR SERS research due to they are small in size and bulk-producible, as well as their easy preparation and tunable surface plasmon resonance (SPR) band in NIR region which is essential to promote the sensitivity of SERS nanotags.[12, 14, 29-31] GNRs were prepared in an aqueous solution using a seedless growth technique developed by El-Sayed and co-workers.[32] Two kinds of GNR-CP core-shell nanostructures were synthesized *via* a facile, one-pot and low-cost oxidative polymerization using pyrrole or aniline as the CP precursor and ferric chloride or ammonium persulfate as the oxidizing agent. The transmission electron microscopy (TEM) images show the rod-shaped GNRs with average length and width of 42.3 ± 6.9 nm and 9.6 ± 1.4 nm, respectively (Fig. 1). Such nanoparticles are considered to show the enhanced permeability and retention effect and long retention in tumor.[33, 34] The UV-vis-NIR absorbance spectrum reveals that these GNRs had a transverse SPR peak at ~515 nm and a longitudinal SPR peak at ~800 nm. Fig. 1b and c display the two kinds of functionalized GNR hybrids, which are wrapped with polyaniline (PANI) and polypyrrole (PPy), respectively. The thickness of CP layers is adjusted to about 7.6 nm for GNR-PANI and 8.9 nm for GNR-PPy, respectively. Obvious red shifts and decrease in absorption peaks are observed in the UV-vis-NIR absorbance spectra of GNR-CPs (Fig. 1d). The nanoprobes also display good dispersion in different physiological environments (Fig. S1†).

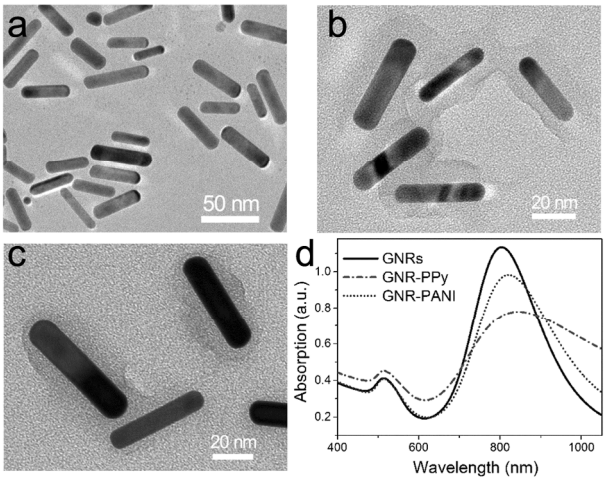

Fig. 1 Characterization of SERS nanoprobes. a-c) TEM images of GNRs, GNR-PANI and GNR-PPy, respectively. d) UV-vis-NIR absorbance spectra of the nanostructures.

The SERS activities of nanoprobes

The SERS fingerprints of GNR-CPs are NIR-excitation-source dependent. No Raman enhancements are observed when the hybrids are irradiated with visible laser (514.5 nm). By contrast, extremely intense SERS signals emerge under NIR laser excitation (785 nm), where the sharp peaks with the highest intensities at 945 cm^{-1} for PPy and 1170 cm^{-1} for PANI (Fig. 2) are attributed to the C–H polaron in-plane deformation and the C–H bending vibration of the quinoid ring, respectively.[35, 36] The core-shell nanostructures are so stable that the SERS signals of CPs remained consistent for five months (Fig. S2†).

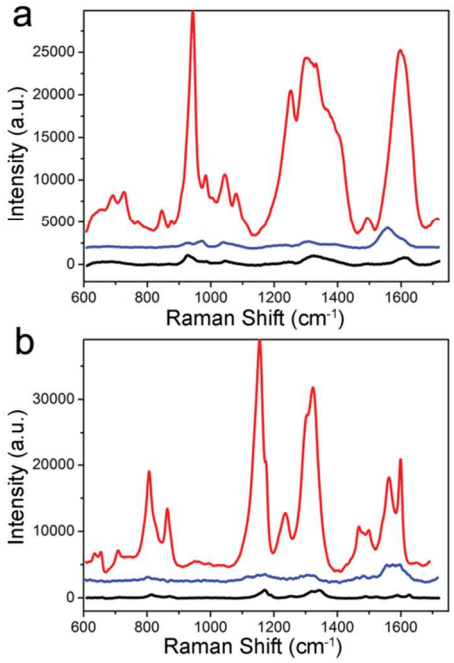

Fig. 2 The Raman spectra of GNR-PPy a) and GNR-PANI b), which exhibit NIR-excitation-source dependent SERS effects. The red and blue lines represent the Raman spectra of GNR-CPs under 785 nm and 514.5 nm laser excitation, respectively. The black lines show the normal Raman spectra of CP molecules.

SERS detection and imaging of tumor cells

With the discovery of prominent and permanent SERS features, we investigated the capabilities of GNR-CPs as new types of NIR SERS tags for the detection and imaging of tumors *in vitro* and *in vivo*. The NIR Raman mapping experiments were conducted by a confocal Raman microspectrometer (Renishaw, InVia) with 785 nm excitation from a semiconductor laser. A549 (adenocarcinomic human alveolar basal epithelial) cells that had been treated with GNR-PPy or GNR-PANI nanoparticles were imaged using the SERS-enhanced absorption signals at 945 cm^{-1} (PPy) or 1170 cm^{-1} (PANI), respectively. Cells incubated with GNRs were set as the control, and the SERS images were acquired using the integrated intensity from 600 to 1700 cm^{-1}, which displayed an ambiguous signal distribution due to the sporadic and weak vibrational signatures of cellular components induced by GNRs (Fig. 3a-c). However, distinguishable SERS images are obtained from the A549 cells incubated with GNR-PANI (Fig. 3e-g) and GNR-PPy (Fig. 3h-j), and the images are closely correlated with the bright-field microscope images. The overlap images of the SERS images and the bright-field images indicate that the tags after endocytosis are located almost exclusively in the cytoplasm. The representative Raman frequencies of CPs can be observed clearly in the scattering lines collected from the cytoplasmic compartments (Fig. 3d), revealing the availability of SERS probes in complex cellular environment. The capability of GNR-CPs as NIR nanotags for cellular SERS imaging is also confirmed in the 4T1 breast adenocarcinoma cells (Fig. S3†). Furthermore, cancer cells were incubated with a mixture of the two probes to demonstrate the multiplexing capabilities of GNR-CPs under a single NIR laser excitation. Fig. 3l and m demonstrate two SERS components and their correlating signal intensity distribution the A549 cell. It must be noted that each mapping is non-interfering which can be ascribed to the narrow spectral features of Raman peaks. To validate the capacity of this new SERS nanotags in more complex biological systems, GNR-CPs were injected into Balb/c

mice bearing xenografts generated from 4T1 breast adenocarcinoma cells. Intense Raman signals that are ascribed to the nanoprobes can be clearly distinguished from the distinctive Raman fingerprint of tumor tissue (Fig. 4), indicating the potential of GNR-CPs as effective SERS probes for detection of tumors *in vivo*.

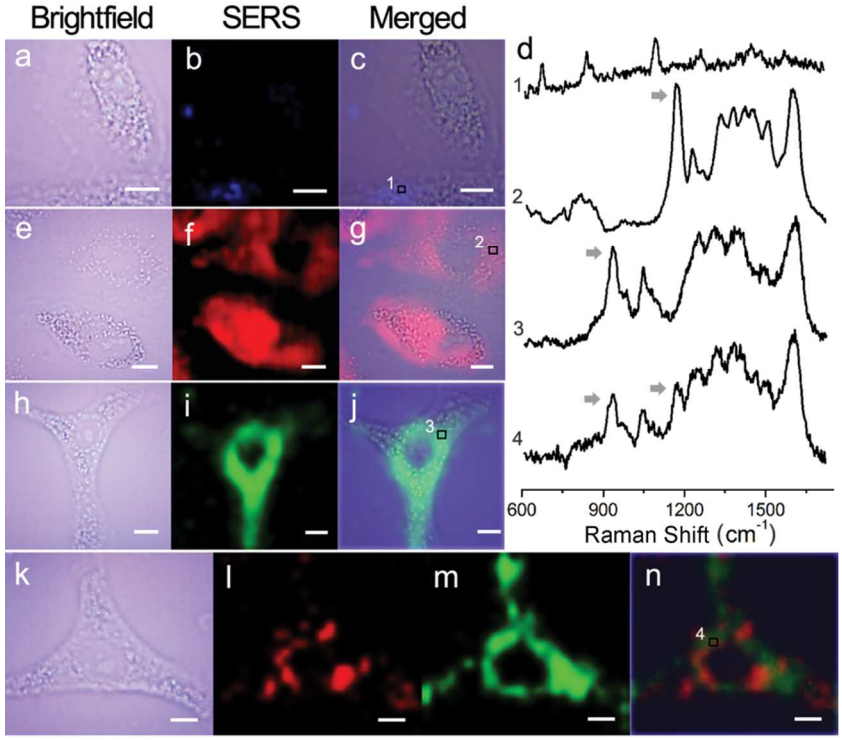

Fig. 3 NIR SERS imaging of A549 cells using GNR-CPs as novel probes. The images are acquired after incubation with GNRs (a-c), GNR-PANI (e-g) or GNR-PPy (h-j) for 4 h. d) shows the Raman spectral lines of the different spots marked in the cytoplasmic compartments. The arrows indicate the Raman peaks used for SERS imaging. k-n) Two-color imaging of a typical A549 cell after incubation with a mixture of two tags (brightfield image (k), GNR-PANI (l), GNR-PPy (m), merged image (n)). Scale bar: 10 μm.

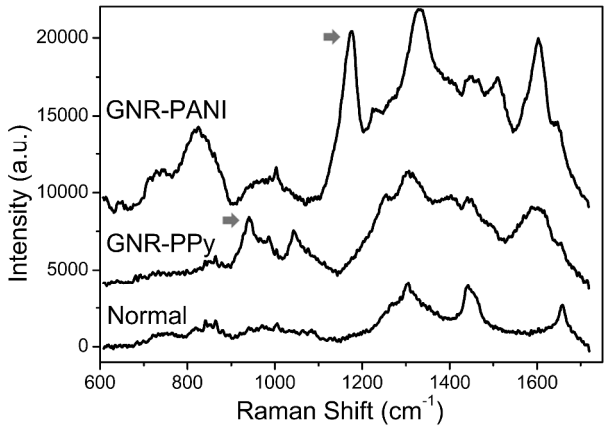

Fig. 4 *In vivo* SERS spectra obtained from xenograft tumor-bearing mice injected with GNR-CP SERS nanotags. Raman spectra were collected from tumor region injected with GNR-PANI (top), GNR-PPy (middle) and normal dorsal region (bottom). The arrows indicate the distinctive SERS peaks of GNR-CPs.

Cytotoxicity assessments of SERS nanotags

The ideal SERS probe should be nontoxic or low-toxic and structural stable under storage or laser irradiation. The cytotoxicities of GNR-CPs were evaluated by classic methyl thiazolyl tetrazolium (MTT) viability assay. A remarkable dose-dependent cytotoxicity is observed in the A549 cells treated with bare GNRs, while the biocompatibilities of the nanostructures are significantly improved after encapsulation using the CP materials (Fig. 5a). The CP-coated gold nanorods also exhibit excellent structural stability under laser irradiation. In comparison with the UV-vis-NIR absorbance spectrum of GNRs, no obvious decrease is noticed in the spectral line of GNR-PANI or GNR-PPy solution after 30 min of high-power 808 nm laser irradiation (Fig. S4†), indicating that CP-coated nanoparticles may be good alternatives to the traditional silica-based nanomaterials for cancer imaging and therapy.

Photothermal effects of SERS nanotags

It is reasonable to speculate the potential of GNR-CPs for NIR photothermal tumor therapy, due to their photothermal-active elements, gold nanorod and CP nanostructures.[18, 37, 38] Fig. 5b shows the photothermal heating curves of different nanoparticle solutions under laser exposure. In marked contrast to the PBS sample, the gold nanoparticle solutions experience rapid increases of temperature during the NIR exposure. However, the core-shell structures generate heat more efficiently ($\Delta T \approx 65$ ˚C, 5 min) than GNRs. The extraordinary heat-generating capacity of GNR-CPs can be largely attributed to the enhanced photothermal energy conversion efficiency caused by the CP-coating.[25]

In vitro antitumor effects of the nanotags

Next, we used the nanoprobes as the photothermal agents for *in vitro* cancer cell ablation under NIR laser irradiation. Fig. 5c shows the relative viability of A549 cells after laser treatment, which demonstrates dose-dependent anti-proliferative effects. At low

nanoparticle concentration, no obvious cell death is recorded in the GNRs group, while only about 56% and 71% cell viabilities are observed in the cells incubated with GNR-PPy and GNR-PANI, respectively. The inhibition rates reach more than 80% when the nanotags concentrate up to 100 μM, implying remarkable photothermal therapeutic effects *in vitro*. A549 cells were also stained with Hoechst 33258 dye, a DNA-binding fluorochrome, to study the apoptosis of tumor cells after laser treatment. As shown in the fluorescence microscopy images (Fig. 5e), the cells without any treatment display uniform spherical nuclei which emitted light blue fluorescence. No significant morphological change is discovered in the control cells after NIR irradiation. However, irregular granules with bright blue luminescence are observed in the photothermal-treated tumor cells, which can be ascribed to the DNA fragmentation and chromatin condensation during apoptosis. The amount of apoptotic cells in GNR-CPs treated samples are much more than that in the A549 cells incubated with GNRs (Fig. 5d), further confirming the superior photothermal effects of GNR-CPs.

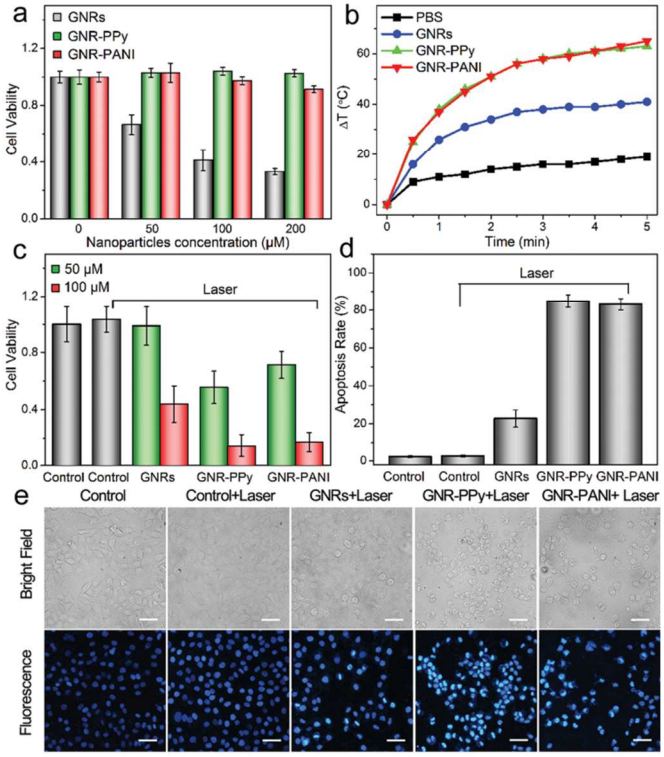

Fig. 5 *In vitro* photothermal ablation of tumor cells. a) Cell viability of A549 cells with 24 h exposure to various gold nanostructure concentrations. b) Photothermal heating curves of PBS with or without nanoparticles exposed to the 808 nm laser at a power density of 2.5 W cm-2. c) A549 cell viability after treatment with different nanoparticles and NIR laser. d) Apoptosis rate of A549 cells after NIR photothermal ablation. e) Fluorescence photomicrographs of A549 cells after photothermal ablation and staining with Hoechst 33258 (Scale bar: 100 μm).

In vivo photothermal therapy

Finally, the *in vivo* therapeutic efficacies of nanotags induced photothermal tumor ablation were investigated. An infrared thermal camera was used to monitor the local temperature during the laser irradiation (Fig. 6a). No significant temperature change is noticed on the tumor injected with PBS (Max: 43.4 ˚C) or GNRs (Max: 45.8 ˚C) during the laser irradiation. In contrast, the surface temperatures of tumor containing GNR-CPs rapidly increase from about 30 to 75 ˚C over the irradiation time, which is fully sufficient to kill the tumor *in vivo*.[39] Indeed, brown necrosis tissues can be easily observed on the tumor regions injected with GNR-PPy or GNR-PANI (Fig. 6d). The *in vivo* therapeutic efficacy of photothermal treatment was evaluated by measuring the tumor size with a digital caliper. Fig. 6b demonstrates the changes of relative tumor volume with respect to time. Mice treated with PBS experience a rapid growth of tumor volume during the 20-day observation period. The tumor sizes of mice injected with GNRs are reduced in the first few days, but the tumors begin to grow again with a similar growth rate to the PBS group in the next days, indicating a low tumor growth inhibition rate induced by GNRs at the experimental concentration. In contrast, highly efficient photothermal treatments are discovered on the mice treated with GNR-CPs. All of the mice in GNR-PPy group and four out of five mice in GNR-PANI group achieve complete tumors ablation, leaving black scars at their original sites with no signs of reoccurrence. And the scars subsequently fall off twenty days after photothermal treatment (Fig. 6d). Tumor of the other mouse in GNR-PANI group is not completely ablated and showed a slow growth after treatment, probably due to a small part of the larger block of tumor tissue free of laser irradiation. The average life spans of mice treated with PBS or GNRs are about 26 days, much lower than those treated with GNR-CPs (Fig. 6c), further demonstrating the excellent *in vivo* therapeutic efficacies of GNR-CPs induced photothermal ablation.

Toxic side effect is a major concern in nanomaterial-based cancer therapy. The body weight of the mice for all groups during post-treatment was measured owing to the high toxicity usually leads to weight loss.[23, 40] As shown in the Fig. 7a, no significant body weight loss is observed in all groups. To accurately assess the long-term systematic toxicities of GNR-CPs, the pathological examinations of major organs collected from GNR-CPs treated mice were carried out at 60 days after laser treatment, because some of the gold nanosturctures were likely to transfer into the major organs after injection.[41, 42] Fig. 7b displays the haematoxylin and eosin (H&E) stained images of major organs including heart, liver, spleen, lung, and kidney, which showed no noticeable organ lesions in the tissue slices, suggesting the promise of using GNR-CPs as biocompatible nanoagents for *in vivo* photothermal therapy.

Experimental Section

Synthesis of SERS nanoprobes

GNRs were prepared in an aqueous solution using a seedless growth technique developed by El-Sayed and co-workers with minor modification.[32] Briefly, 25 mL of cetyltrimethylammonium bromide (CTAB; 0.2 M) was added into $HAuCl_4$ aqueous solution (25 mL, 1 mM) under gentle shaking at room temperature. $AgNO_3$ (0.9 mL, 4 mM) and HCl (50 μL, 37%) were then introduced. Following this, 350 μL of ascorbic acid (78.8 mM) was added to the mixture, which rapidly turned from dark-yellow to colorless. Immediately afterward, 75 μL of ice-cold $NaBH_4$ at the concentration of 0.01 M was injected to the growth solution, and the mixture was finally transferred to a water bath allowing reaction overnight at 28 ˚C. The final product was purified by centrifugation (10000 rpm, 30 min) three times and then resuspended in 25 mL deionized water. GNR-PPy core-shell nanostructures were synthesized according to the following procedure: 10 mL of GNRs solution, 4 mL of 40 mM sodium dodecyl sulfate (SDS), and 400 μL of pyrrole aqueous solution (1%) were mixed gently by hand shaking, and then the mixture then was not disturbed for 3 h. Subsequently, 100 μL of 0.1 M $FeCl_3$ solution was added. After being stirred for 10 s, the reaction solution was placed on a shaker with at a slow speed for 24 h to ensure complete

polymerization. The preparation of GNR-PANI core-shell nanostructures was similar to that of GNR-PPy. In brief, 10 mL of GNRs solution, 2 mL of 40 mM SDS, 200 μL of 2 M HCl and 100 μL of aniline acidic aqueous solution (2.5%) were mixed under vigorous stirring for 1 h. Following this, 50 μL of 1 M ammonium persulfate solution was added, and then the reaction solution was placed on a shaker with at a slow speed for 24 h to ensure complete polymerization. The final products were purified by centrifugation (10000 rpm, 30 min) three times. To enhance the dispersion of the as-prepared GNR-CP nanoparticles in physiological environments, polyvinyl pyrrolidone was simply attached onto the CP shell by hydrogen bond interactions. The as-prepared GNR-PPy or GNR-PANI was then resuspended in 5 mL deionized water and stored at 4 ˚C for further use.

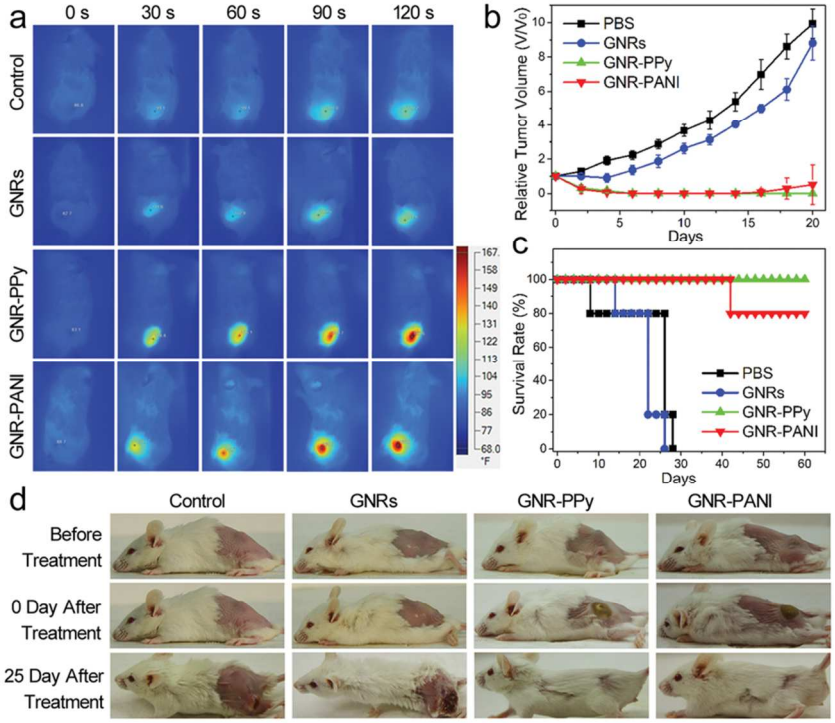

Fig. 6 *In vivo* photothermal therapy of breast tumor. a) Infrared thermal images of tumor-bearing mice exposed to the NIR laser after injection with PBS, GNRs, GNR-PPy and GNR-PANI, recorded at different time intervals. b) Tumor growth curves of different groups of mice after photothermal treatment. c) Survival curves of mice bearing 4T1 tumors after various treatments indicated. d) Representative photographs of tumor-bearing mice.

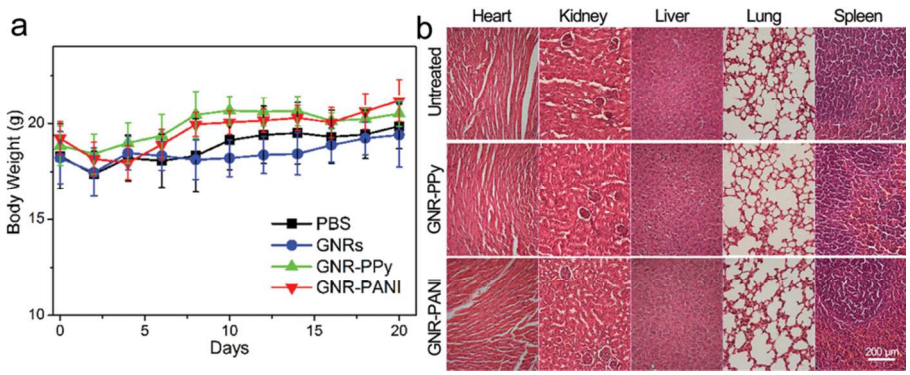

Fig. 7 *In vivo* nanotoxicity of SERS nanotags. a) Mean body weights of mice in various groups after treatment. b) Representative H&E stained images of major organs collected from the mice treated with GNR-CPs at 60 days after laser treatment.

Characterization

TEM analysis was carried out with a JEM-2100HR transmission electron microscope (JEOL, Japan) operated at 200 kV. UV-Vis absorption spectra of the nanostructures were measured by a UV-Vis spectrometer (UV-3200S, MAPADA, Shanghai, China). Raman spectra were collected using a Renishaw inVia microspectrometer (Derbyshire, England) with excitation wavelengths of 514.5 nm and 785 nm generated by an Ar^{+} laser and a semiconductor laser, respectively.

Photothermal heating experiment

GNRs, GNR-PPy and GNR-PANI suspensions were diluted to a final concentration of 100 μM (elemental gold concentration) in phosphate buffered saline (PBS), and then irradiated by a continuous-wave diode NIR laser (808 nm, Changchun New Industries Optoelectronics Technology, China) with a power density of 2.5 W cm^{-2} for 5 min. The temperatures of the solutions were measured every 30 s using a thermocouple thermometer. To evaluate

the structural stabilities of gold nanostructures under laser irradiation, the samples were irradiated with 808 nm laser for 30 min, and the UV-vis-NIR absorbance spectra were measured at 10 min and 30 min by a spectrophotometer.

Tumor model

Adenocarcinomic human alveolar basal epithelial (A549) cells were used for in vitro experiments. The cells were cultured in DMEM medium supplemented with 10% FBS, penicillin (100 units mL^{-1}), and streptomycin (100 mg mL^{-1}) in 5% CO_2 and 95% air at 37 ˚C in a humidified incubator. Female albino Balb/c mice (5-6 weeks old) were purchased from Laboratory Animal Center, South China Medical College, and performed under protocols approved by South China Normal University Animal Care and Use Committee. 4T1 mammary carcinoma cells were cultured in RIPM-1640 medium containing 10% FBS, penicillin (100 units mL^{-1}), and streptomycin (100 mg mL^{-1}) in 5% CO_2 and 95% air at 37 ˚C in a humidified incubator. Then the cells were harvested and resuspended in the PBS at the concentration of 2×10^7 cells per mL. 100 μL of cell suspensions were subcutaneously injected into the flank regions in female Balb/c mice. Animal experiments started when the tumor size reached approximately 200 mm^3.

NIR SERS detection and imaging

For in vitro Raman imaging, A549 cells precultured in DMEM medium were seeded onto quartz substrates in cell culture petri dishes (35 mm) with 2 mL of medium for 24 h to reach 70-80% confluence. Then the growth medium was replaced with the DMEM medium containing GNRs, GNR-PPy or GNR-PANI at the concentration of 100 μM (elemental gold concentration). After incubation at 37 ˚C for 4 h, the cells were rinsed with PBS five times and then fixed with 4% formalin buffered in PBS for 10 min. Raman imaging was carried out using a Renishaw inVia confocal Raman system (controlled by WiRE 3.2 software) coupled to a Leica DM-2500M microscope. The spectrometer was equipped with a 785 nm semiconductor laser. A 50× objective lens (~1 μm laser spot size) was used to focus the laser beam and to collect the Raman signal. Raman spectral mapping was performed in a Streamline mode at 5 s integration time at wavenumber center 1200 cm^{-1}. For in vivo Raman detection, 4T1-bearing mice were injected with 100 μL of GNR-PPy or GNR-PANI (dose = 4 mg kg^{-1}). After that, mice were anaesthetized with 4% chloral hydrate (0.1 mL 10 g^{-1}). Raman measurements were conducted by the Renishaw inVia confocal Raman microscope equipped with a 785 nm semiconductor laser. A 20× objective lens was used and the laser spot was about 3 μm in diameter. The Raman spectral lines were recorded in static mode for a 30 s laser exposure over a wavenumber range of 600-1700 cm^{-1}.

NIR Photothermal therapy

A549 cells were plated into 96-well plates at a density of 5×10^4 cells per well and allowed to adhere prior to addition of various concentrations of GNRs, GNR-PPy and GNR-PANI. After 4 h of incubation at 37 ˚C, the cells were irradiated with the NIR laser (808 nm, 2.5 W cm^{-2}) for 1.5 min and then incubated at 37 ˚C for a further 24 h. A standard MTT assay was performed to evaluate cell viability according to the manufacturer's suggested procedures. For fluorescence analysis, A549 cells were seeded onto sterile glass coverslips in cell culture petri dishes (35 mm) with 2 mL of medium for 24 h to reach 70-80% confluence. Then the culture medium was removed, followed by incubation with DMEM medium containing gold nanostructures at the concentration of 100 μM for 4 h. After that, cells were irradiated with the 808 nm laser for 5 min and then incubated at 37 ˚C for an additional 2 h. Afterward, cells were washed three times with PBS and then fixed with 4% formalin buffered in PBS for 10 min. After washing three times with PBS, A549 cells were stained with Hoechst 33258 dye (4 μg mL^{-1}) for 10 min. The apoptotic cells were observed using a fluorescence microscopy (Leica DM-2500, Leica Microsystems, Wetzlar, Germany). For in vivo photothermal therapy, mice bearing 4T1 tumors were intratumorally injected with 100 μL of GNRs, GNR-PPy or GNR-PANI (five mice per group, dose = 4 mg kg^{-1}). Mice injected with PBS (100 μL) were set as the control. NIR laser irradiation (808 nm, 2.5 W cm^{-2}, 2 min) was carried out only one time 24 h after injection. The surface temperature of tumor during the laser irradiation was monitored using an infrared thermal camera (Fluke Ti 200, Fluke Corp, Everett, Washington, USA). The tumor sizes were measured by a digital caliper every other day and calculated as the volume = (tumor length) × (tumor width)^2 /2. Relative tumor volumes were calculated as V/V_0 (V_0 was the tumor volume when the treatment was initiated).

Cytotoxicity assessment and histological examination

To assess the cell toxicities of gold nanostructures, A549 cells pre-cultured in 96-well plates were incubated in DMEM culture medium containing different concentrations of GNRs, GNR-PPy and GNR-PANI for 24 h. Then the cell viability was measured by the MTT assay. For investigation of the in vivo nanotoxocity of GNR-CPs, The body weight of the mice for all groups during post-treatment was measured. To accurately assess the long-term systematic toxicities of GNR-CPs, nanoprobe-treated mice were sacrificed 60 days after treatment, and the major organs (heart, liver, spleen, lung and kideny) of those mice were then collected, fixed in 4% neutral formaldehyde, conducted with paraffin embedded sections, stained with hematoxylin and eosin, and observed under a digital microscope (Leica DM-2500, Leica Microsystems).

Conclusion

In summary, we have demonstrated a noval strategy for fabrication of NIR SERS nanoprobes, using conducting polymer as the bifunctional Raman active molecule. In comparison with the traditional metal substrate-dye-silica structure, the synthetic method of these dye-free SERS nantags is extremely simple and inexpensive. Two SERS nanoprobes, GNR-PPy and GNR-PANI, have been fabricated *via* facile oxidative polymerizations. The GNR-CP core-shell nanostructures display interesting NIR-excitation-source dependent SERS activities, and the application of GNR-CPs as promising novel NIR SERS nanoprobes for fast tumor imaging *in vitro* and *in vivo* has been achieved in cultured cancer cells and tumor-bearing mice. GNR-CPs also reveal remarkably improved structural stability, biocompatibility, and NIR photothermal energy conversion efficiency in comparison with the bare gold nanorods, which promote the practical application of GNR-CPs for high-performance photothermal therapy *in vitro* and *in vivo*. The theranostic applications of these novel NIR SERS nanotags will help establish an efficient strategy for imaging-guided cancer therapy.

Acknowledgements

This work is supported by the National Natural Science Foundation of China (61335011, 61275187, 11404116 and 31300691), Specialized Research Fund for the Doctoral Program of Higher Education of China (20114407110001 and 20134407120003), the Natural Science Foundation of Guangdong Province of China (2014A030310306 and 2014A030311024), the Science and Technology Project of

Guangdong Province of China (2012A080203008), the Science and Technology Innovation Project of the Education Department of Guangdong Province of China (2013KJCX0052), and the Scientific Research Cultivation Fund for Young Teachers of South China Normal University (14KJ10).

Notes and references

MOE Key Laboratory of Laser Life Science & SATCM Third Grade Laboratory of Chinese Medicine and Photonics Technology, College of Biophotonics, South China Normal University, Guangzhou, Guangdong 510631, PR China. E-mail: liuzm021@126.com; ann@scnu.edu.cn.

† Electronic Supplementary Information (ESI) available. See DOI: 10.1039/b000000x/

1 A. Huefner, W. L. Kuan, R. A. Barker and S. Mahajan, *Nano Lett.*, 2013, **13**, 2463-2470.
2 D. Zhu, Z. Wang, S. Zong, H. Chen, X. Wu, Y. Pei, P. Chen, X. Ma and Y. Cui, *Nanoscale*, 2014, **6**, 8155-8161.
3 M. Li, S. K. Cushing, J. Zhang, S. Suri, R. Evans, W. P. Petros, L. F. Gibson, D. Ma, Y. Liu and N. Wu, *ACS Nano*, 2013, **7**, 4967-4976.
4 Z. Chen, S. M. Tabakman, A. P. Goodwin, M. G. Kattah, D. Daranciang, X. Wang, G. Zhang, X. Li, Z. Liu, P. J. Utz, K. Jiang, S. Fan and H. Dai, *Nat. Biotechnol.*, 2008, **26**, 1285-1292.
5 K. V. Kong, W. K. Leong, Z. Lam, T. X. Gong, D. Goh, W. K. O. Lau and M. Olivo, *Small*, 2014, **10**, 5030-5034.
6 K. V. Kong, Z. Lam, W. D. Goh, W. K. Leong and M. Olivo, *Angew. Chem. Int. Ed.*, 2012, **51**, 9796-9799.
7 W. W. Zhang, Y. Q. Wang, X. Y. Sun, W. H. Wang and L. X. Chen, *Nanoscale*, 2014, **6**, 14514-14522.
8 K. K. Maiti, U. S. Dinish, A. Samanta, M. Vendrell, K.-S. Soh, S.-J. Park, M. Olivo and Y.-T. Chang, *Nano Today*, 2012, **7**, 85-93.
9 A. Samanta, K. K. Maiti, K.-S. Soh, X. Liao, M. Vendrell, U. S. Dinish, S.-W. Yun, R. Bhuvaneswari, H. Kim, S. Rautela, J. Chung, M. Olivo and Y.-T. Chang, *Angew. Chem. Int. Ed.*, 2011, **50**, 6089-6092.
10 U. S. Dinish, G. Balasundaram, Y. T. Chang and M. Olivo, *Sci. Rep.*, 2014, **4**, 4075.
11 X. Qian, X. H. Peng, D. O. Ansari, Q. Yin-Goen, G. Z. Chen, D. M. Shin, L. Yang, A. N. Young, M. D. Wang and S. Nie, *Nat. Biotechnol.*, 2008, **26**, 83-90.
12 G. von Maltzahn, A. Centrone, J. H. Park, R. Ramanathan, M. J. Sailor, T. A. Hatton and S. N. Bhatia, *Adv. Mater.*, 2009, **21**, 3175-3180.
13 X. Wang, C. Wang, L. Cheng, S. T. Lee and Z. Liu, *J. Am. Chem. Soc.*, 2012, **134**, 7414-7422.
14 Y. Zhang, J. Qian, D. Wang, Y. Wang and S. He, *Angew. Chem. Int. Ed.*, 2013, **52**, 1148-1151.
15 X. J. Liu, Q. Wang, C. Li, R. J. Zou, B. Li, G. S. Song, K. B. Xu, Y. Zheng and J. Q. Hu, *Nanoscale*, 2014, **6**, 4361-4370.
16 J. Yang, D. Shen, L. Zhou, W. Li, J. Fan, A. M. El-Toni, W.-x. Zhang, F. Zhang and D. Zhao, *Adv. Healthcare Mater.*, 2014, **3**, 1620-1628.
17 G. A. Sotiriou, F. Starsich, A. Dasargyri, M. C. Wurnig, F. Krumeich, A. Boss, J.-C. Leroux and S. E. Pratsinis, *Adv. Funct. Mater.*, 2014, **24**, 2818-2827.
18 Z. Zha, X. Yue, Q. Ren and Z. Dai, *Adv. Mater.*, 2013, **25**, 777-782.
19 K. Yang, H. Xu, L. Cheng, C. Sun, J. Wang and Z. Liu, *Adv. Mater.*, 2012, **24**, 5586-5592.
20 E. Ju, Z. Li, M. Li, K. Dong, J. Ren and X. Qu, *Chem. Commun.*, 2013, **49**, 9048-9050.
21 J. Zhou, Z. Lu, X. Zhu, X. Wang, Y. Liao, Z. Ma and F. Li, *Biomaterials*, 2013, **34**, 9584-9592.
22 J. Yang, J. Choi, D. Bang, E. Kim, E.-K. Lim, H. Park, J.-S. Suh, K. Lee, K.-H. Yoo, E.-K. Kim, Y.-M. Huh and S. Haam, *Angew. Chem. Int. Ed.*, 2011, **50**, 441-444.
23 Y. Yuan, Z. Wang, P. Cai, J. Liu, L.-D. Liao, M. Hong, X. Chen, N. Thakor and B. Liu, *Nanoscale*, 2015, **7**, 3067-3076.
24 C. Wang, H. Xu, C. Liang, Y. Liu, Z. Li, G. Yang, L. Cheng, Y. Li and Z. Liu, *ACS Nano*, 2013, **7**, 6782-6795.
25 J. Li, J. Han, T. Xu, C. Guo, X. Bu, H. Zhang, L. Wang, H. Sun and B. Yang, *Langmuir*, 2013, **29**, 7102-7110.
26 Q. Tian, Q. Wang, K. X. Yao, B. Teng, J. Zhang, S. Yang and Y. Han, *Small*, 2014, **10**, 1063-1068.
27 M. Lin, C. Guo, J. Li, D. Zhou, K. Liu, X. Zhang, T. Xu, H. Zhang, L. Wang and B. Yang, *ACS Appl. Mater. Interfaces*, 2014, **6**, 5860-5868.
28 Y. Jin, Y. Li, X. Ma, Z. Zha, L. Shi, J. Tian and Z. Dai, *Biomaterials*, 2014, **35**, 5795-5804.
29 L. Jiang, J. Qian, F. Cai and S. He, *Anal. Bioanal. Chem.*, 2011, **400**, 2793-2800.
30 J. V. Jokerst, A. J. Cole, D. Van de Sompel and S. S. Gambhir, *ACS Nano*, 2012, **6**, 10366-10377.
31 J. Qian, L. Jiang, F. Cai, D. Wang and S. He, *Biomaterials*, 2011, **32**, 1601-1610.
32 M. R. Ali, B. Snyder and M. A. El-Sayed, *Langmuir*, 2012, **28**, 9807-9815.
33 S. Nie, *Nanomedicine (Lond)*, 2010, **5**, 523-528.
34 S. D. Perrault, C. Walkey, T. Jennings, H. C. Fischer and W. C. W. Chan, *Nano Lett.*, 2009, **9**, 1909-1915.
35 X. Wan, X. Liu, G. Xue, L. Jiang and J. Hao, Polymer, 1999, 40, 4907-4914.
36 T.-M. Wu and Y.-W. Lin, *Polymer*, 2006, **47**, 3576-3582.
37 L. Cheng, C. Wang, L. Z. Feng, K. Yang and Z. Liu, *Chem. Rev.*, 2014, **114**, 10869-10939.
38 N. Li, P. Zhao and D. Astruc, *Angew. Chem. Int. Ed.*, 2014, **53**, 1756-1789.
39 B. Jang, J. Y. Park, C. H. Tung, I. H. Kim and Y. Choi, *ACS Nano*, 2011, **5**, 1086-1094.
40 W. Zhang, Z. Guo, D. Huang, Z. Liu, X. Guo and H. Zhong, *Biomaterials*, 2011, **32**, 8555-8561.
41 M. A. El-Sayed, A. A. Shabaka, O. A. El-Shabrawy, N. A. Yassin, S. S. Mahmoud, S. M. El-Shenawy, E. Al-Ashqar, W. H. Eisa, N. M. Farag, M. A. El-Shaer, N. Salah and A. M. Al-Abd, *PLoS ONE*, 2013, **8**, e76207.
42 S. M. Lee, H. Park and K. H. Yoo, *Adv. Mater.*, 2010, **22**, 4049-4053.